Reaction products and the X-ray structure of AmpDh2, a virulence determinant of *Pseudomonas aeruginosa*

Siseth Martínez-Caballero,[§] Mijoon Lee,[#] Cecilia Artola-Recolons,[§] César Carrasco-López,[§] Dusan Hesek,[#] Edward Spink,[#] Elena Lastochkin,[#] Weilie Zhang,[#] Lance M. Hellman,[#] Bill Boggess,[#] Shahriar Mobashery*,[#] and Juan A. Hermoso*,[§]

[§]Department of Crystallography and Structural Biology, Inst. Química-Física "Rocasolano", CSIC, Serrano 119, 28006 Madrid, Spain [#]Department of Chemistry and Biochemistry, Nieuwland Science Hall, Notre Dame, Indiana 46556, United States

Supporting Information

Contents

Experimental Procedures.

Sedimentation Velocity Experiments. Sedimentation velocity experiments were performed in an XL-I analytical ultracentrifuge instrument (Beckman Coulter). The loading concentration of AmpDh2[1] was 3.1 μM in 20 mM sodium phosphate buffer, 0.1 M sodium chloride, pH 7.1. Sedimentation velocity experiment was performed at 25,000 rpm at 4 ºC using the AN-TI 60 rotor. Protein absorbance was measured at 280 nm. Data were fit using numerical solutions of the Lamm equation using the SEDFIT program.[2] Values were obtained with a 95% confidence interval.

The experimentally obtained s values were converted to standard 20 ºC, water conditions ($s_{20,w}$) using equation 1.

$$s_{20,w} = s_{T,B} \cdot \frac{(1-\bar{v}\rho_{20,w}) \cdot (\eta_{T,B})}{(1-\bar{v}\rho_{T,B}) \cdot (\eta_{20,w})} \qquad (1)$$

Where $s_{T,B}$ is the s value in the experimental temperature and buffer, $\bar{v}$ is the partial specific volume (0.7387 mL g^{-1} for AmpDh2), $\rho_{T,B}$ is the buffer density at experimental temperature, $\rho_{20,w}$ is the water density, $\eta_{T,B}$ is the buffer viscosity at experimental temperature and $\eta_{20,w}$ the water viscosity. The $\bar{v}$, density and viscosity values for the experimental buffer were calculated using SEDNTERP.[3]

Sedimentation Equilibrium Experiments. The loading concentration of AmpDh2 was 4.9 μM in 20 mM sodium phosphate buffer, 0.1 M sodium chloride, pH 7.1. Sedimentation equilibrium experiments were run at centrifuge speeds of 20,000 and 25,000 rpm at 4 ºC. Samples were considered to have reached equilibrium when two scans taken 6 hours apart were superimposable. Data were fit using equation 2.

$$A(r) = \alpha_n exp[\sigma_n(r^2 - r_o^2)] + \zeta \qquad (2)$$

Where A(r) is the absorbance at radial position r, α_n is the absorbance of protein (n) at r_o, ζ is the baseline offset and σ_n is the effective reduced molecular weight. The effective reduced molecular weight is calculated using equation 3.

$$\sigma_n = M_n(1 - \bar{v}_n\rho)\omega^2/2RT \qquad (3)$$

Where M_n is the molecular weight of the protein n, $\bar{v}_n$ is the partial specific volume of the protein, ρ is the solvent density, ω is the angular velocity, R is the gas constant and T is the absolute temperature in Kelvin.

Reaction of AmpDh2/MltA with the bacterial sacculus. The sacculus of *P. aeruginosa* PA01 was isolated by the general procedure described previously.[1, 4] Each reaction mixture contained 140 μL of the sacculus preparation and 0.9 μM of AmpDh2 in 20 mM phosphate, pH 8.0, and was incubated at 37 °C on an orbital shaker. The reactions were stopped after 24 h of incubation by boiling of the mixture for 3 min. Each reaction mixture was concentrated under reduced pressure. The residue was reconstituted in 400 μL of 10 mM acetate buffer with 10 mM $MgCl_2$, pH 4.0 and MltA (1.25 μM) was added. The resulting mixture was incubated at 37 °C for 4 h. The mixture was boiled for 3 min and was concentrated under reduced pressure. The residue was taken up into water and the resulting suspension was centrifuged. The supernatant was separated and was used for analysis by LC/MS or LC/MS/MS.

Liquid Chromatography/Mass Spectrometry. LC/MS and LC/MS/MS conditions were described previously.[4] Briefly, the Bruker electrospray ionization source was operated in the positive ion mode with the following parameters: end plate offset voltage = –500 V, capillary voltage = 2000 V, and nitrogen was used as both a nebulizer (4 bar) and dry gas (6.0 L/min flow rate at 200 ºC temperature). LC separations were performed on a Dionex Acclaim™ PolarAdvantage II C18 column with the mobile-phase gradient consisting of elution at 0.5 mL/min with 98% A/2% B for 5 min, followed by a 40-min linear gradient to 83% A/17% B (A = 0.1% formic acid in water; B = 0.1% formic acid in acetonitrile).

Quantification. Peak areas from extracted-ion chromatograms of the corresponding *m*/*z* values were integrated and normalized to the internal standard (compound **11**).[5] Amounts of reaction products were calculated as a percentage of the total peak area of products found. Total peak areas included the contributions from peak areas of charge states +1, +2, +3, +4, and +5, when present.

Chart S1. Chemical Structures of Compounds Used in This Study.

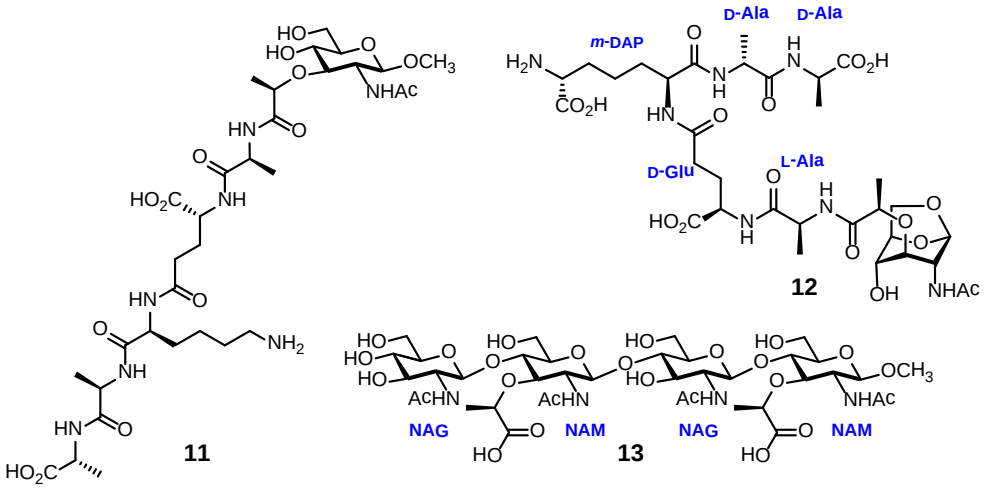

Synthesis of Compounds. Compounds **11** and **12** were prepared according to the literature methods developed by our laboratory.[5, 6] Compound **14** (below) was prepared from D-glucosamine in 40 convergent steps according to a literature procedure.[7]

β-Methyl 2-acetamido-2-deoxy-β-D-glucopyranosyl-(1→4)-2-acetamido-3-*O*-((*R*)-1´-carboxyethyl)-2-deoxy-β-D-glucopyranosyl-(1→4)-2-acetamido-2-deoxy-β-D-glucopyranosyl-(1→4)-2-acetamido-3-*O*-((*R*)-1´-carboxyethyl)-2-deoxy-β-D-glucopyranoside (β-methyl NAG-NAM-NAG-NAM, 13). Compound **14** (150 mg, 0.10 mmol) was dissolved in AcOH (3 mL) and the solution was stirred at 80 ºC for 1 h. Methanol (3 mL) and 10% Pd/C (0.10 g) and were added to the reaction mixture and the suspension was stirring for 18 h. The reaction mixture was filtered through a layer of Celite and the residue was washed with MeOH. The combined filtrate was concentrated to dryness under reduced pressure. The HPLC purification (Sunfire C18, 100 Å, 19 × 150 mm using a linear gradient from 2 to 20% acetonitrile in water supplemented with 0.1% TFA over 20 min) of the crude product gave the desired tetrasaccharide (45 mg, 46%). ^{1}H NMR (500 MHz, D_2O) δ 1.42, 1.44 (2 × d, *J* = 7.0 Hz, 6H; 2Lac-CH_3), 1.98, 2.02, 2.07 (3 × s, 12H; 4NHCOCH_3), 3.36 - 3.95 (m, 24H), 3.46 (s, 3H; OCH_3), 4.38 (d, *J* = 8.2 Hz, 1H), 4.47 - 4.57 (m, 5H); ^{13}C NMR (126 MHz, D_2O) δ 18.4, 18.5 (2 × q, 2Lac-CH_3), 22.2, 22.45, 22.47, 22.49 (4 × q, NHCOCH_3), 54.7 (d), 55.0 (d), 55.5 (d), 56.2 (d), 57.2

(q, OCH_3), 59.9 (t), 60.0 (t), 60.6 (t), 61.4 (t), 70.5 (d), 72.3 (d), 73.7 (d), 74.9 (d), 75.2 (d), 75.4 (d), 76.4 (d), 77.6, 77.7 (2 × d, 2Lac-α-C), 79.9 (d), 80.0 (d), 80.1 (d), 100.2 (d), 100.3 (d), 101.7 (d), 102.1 (d), 174.61, 174.68, 174.74, 174.8, 177.6, 177.7; HRMS (ESI), calcd for $C_{39}H_{64}N_4O_{25}$ ($M+H^+$), 989.3932, found 989.3897.

Scheme S1. Synthesis of the tetrasaccharide **13**.

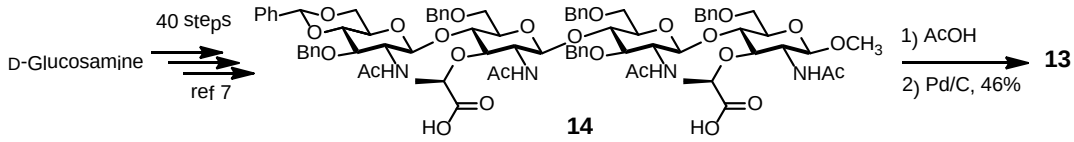

Crystallization. Prior to crystallization, the purified AmpDh2 was dialyzed against citrate buffer (20 mM, pH 5.0) and concentrated to 8 mg/mL. Crystallization trials were set up at 291 K using the sitting-drop vapor-diffusion method. Good quality crystals were grown in 0.2 M potassium thiocyanate, 0.1 M bis-tris propane (1,3-bis(tris(hydroxymethyl)methylamino)propane), pH 7.5 and 18% PEG 3350. The mixture consisted of equal volumes of protein with precipitant solution (1 μL) and equilibrated against 500 μL of the reservoir solution. The crystals were soaked into cryoprotectant solution (paratone/paraffin oil, proportion 7:3), before flash cooling at 100 K. The complex of AmpDh2 with L-Ala-γ-D-Glu-*m*-DAP-D-Ala (AmpDh2:5P complex) was obtained by soaking native crystals in a 15 mM solution of compound **12** mixed with the crystallization condition (18% PEG 3350, 0.1 M bis-tris propane, pH 7.5, 0.2 M potassium thiocyanate). The crystals were soaked in paratone with cryoprotectant solution before flash cooling at 100 K. The complex of AmpDh2 with β-methyl NAG-NAM-NAG-NAM (**13**, AmpDh2:4S complex) was obtained by soaking native crystals in a 40 mM solution of compound **13** mixed with the crystallization condition (18% PEG 3350, 0.1 M bis-tris propane, pH 7.5, 0.2 M potassium thiocyanate). The crystals were soaked in paratone/paraffin oil before flash cooling at 100 K.

Data collection and processing. X-ray diffraction data set for AmpDh2 crystal were collected on beamline PX at the Swiss Light Source (SLS) Villigen, Switzerland. The data set was processed using XDS[8] and scaled using SCALA from CCP4[9] program suite. AmpDh2 crystallized in space group $P2_12_12_1$, with unit cell parameters a = 48.76, b = 100.42, c = 104.26 Å. For the AmpDh2:5P complex a complete X-ray diffraction data set was collected using synchrotron radiation source at the Swiss Light Source (SLS), using a Pilatus 6M detector and fixed wavelength of 1.0064 Å. Collected images were indexed, integrated using XDS and scaled with SCALA. Crystals of AmpDh2:5P complex belonged to the orthorhombic space group $P2_12_12_1$ with cell dimensions of a = 47.63, b = 97.23, c = 104.17 Å, $\alpha = \beta = \gamma = 90°$, and two monomers in the asymmetric unit. For the AmpDh2:4S complex a complete X-ray diffraction data set was collected using synchrotron radiation source at the ESRF (Grenoble, France) in beamline ID29, using a Pilatus 6M detector and fixed wavelength of 0.9716 Å. Collected images were indexed, integrated and scaled using IMOSFLM and SCALA. Crystals of AmpDh2:4S complex belonged to the orthorhombic space group $P2_12_12_1$ with cell dimensions of a = 45.23, b = 93.56, c = 104.35 Å, $\alpha = \beta = \gamma = 90°$, and two monomers in the asymmetric unit.

Structure solution and refinement. AmpDh2 structure was determined by the Molecular Replacement method using the coordinates of native *E. coli* zinc-dependent amidase AmiD (PDB entry 2wkx)[10] as a search model. The rotational and translational searches were performed with the program Phaser from CCP4.[9] The model was manually completed using Coot[11] and was refined with PHENIX.[12]

The R_{work} converged to 0.17 and the R_{free} to 0.21 in the final model. A summary of the refinement statistics is given in Table S1. The complex AmpDh2:5P was solved at 1.7 Å resolution using the Molecular Replacement method with the AmpDh2 structure using MOLREP.[13] The initial model was refined using Phenix.[14] Final values for R_{work} and R_{free} are 0.15 and 0.18 respectively. There is almost no difference between the structure of the native protein and the one with the complex. For AmpDh2:5P, the rmsd value for the Cα compared to the native structure is 0.203 Å for chain A and 0.241 Å for chain B. The product L-Ala-γ-D-Glu-*m*-DAP-D-Ala was clearly identified in the active site of AmpDh2. All of the amino-acid residues in the structure fit perfectly in the Ramachandran plot. The complex AmpDh2:4S was solved at 2.7 Å resolution by Molecular Replacement with MOLREP and refined with REFMAC5.[15] Final values for R_{work} and R_{free} are 0.23and 0.29, respectively. In the case of AmpDh2:4S, the rmsd value for the Cα compared to the native structure is 0.434 Å for chain A and 0.389 Å for chain B. The ligand β-methyl NAM-NAG-NAM-NAG was refined with full occupancy and all of the residues fit perfectly in the Ramachandran plot. Data refinement results are summarized in Table S1.

Table S1. Data collection and refinement statistics*

	AmpDh2	AmpDh2:5P complex	AmpDh2:4S complex
Diffraction data statistics			
Wavelength (Å)	1.00002	1.0064	0.9716
Space group	$P2_12_12_1$	$P2_12_12_1$	$P2_12_12_1$
a, b, c (Å)	48.76, 100.42, 104.26	47.63, 97.23, 104.17	45.23, 93.56, 104.35
α=β=γ	90	90	90
Resolution range (Å)	48.76-1.72 (1.81-1.72)	47.63-1.70 (1.79-1.7)	95.56-2.70 (2.85-2.7)
Unique reflections	54928 (5231)	54041 (7773)	9693 (1089)
Completeness (%)	99.78 (96.46)	100.0 (100.0)	77.0 (60.6)
Redundancy	10.3 (10.8)	13.1 (12.5)	4.2 (3.9)
R_{merge}	0.08 (0.56)	0.08 (0.94)	0.13 (0.65)
Average I/σ(I)	28 (4.6)	17.3 (3.1)	9.0 (2.6)
Refinement statistics			
Resolution range (Å)	46.27-1.72 (1.78-1.72)	47.63-1.70 (1.79-1.70)	93.56-2.70 (2.85-2.70)
R_{work}/R_{free}	0.17/0.20	0.15/0.18	0.23/0.29
No. Atoms			
Protein	3915	3868	3818
Water	871	464	42
Ligand	13	66	70
B-factor (Å^2)			28.7
Protein	18.20	28.60	46.80
Water	27.15	35.80	28.80
Ligand	16.64	33.70	119.3
R.m.s. deviations			
Bond length (Å)	0.007	0.011	0.017
Bond angles (°)	1.14	1.47	1.76
Ramachandran favored/outliers (%)	98.0/0.0	98.0/0.2	95.0/0.4
Residues in the AU	490	486	482
PDB code	4bj4	4bol	4bpa

*Values between parentheses correspond to the highest resolution shells

Table S2. Polar interactions involved in AmpDh2 dimerization

Nº	Residue (monomer B)	Distance (Å)	Residue (monomer A)
Hydrogen bonds			
1	ARG 76[N]	2.98	ASN 24[O]
2	SER 61[OG]	2.72	ASN 31[O]
3	ARG 82[NH2]	3.57	GLN 32[O]
4	ARG 82[NE]	3.01	GLN 32[OE1]
5	ARG 76[N]	2.98	ASN 24[O]
6	TRP 85[NE1]	3.60	ASP 33[OD1]
7	ARG 83[NH2]	2.87	ASP 33[OD2]
8	ARG 83[N]	2.73	ASP 33[O]
9	SER 29[OG]	3.78	THR 56[O]
10	ALA 30[N]	2.95	THR 56[O]
11	ASN 24[N]	2.87	VAL 74[O]
12	SER 29[N]	2.91	LEU 77[O]
13	ARG 35[NE]	2.92	GLU 80[O]
14	ARG 35[NH1]	2.91	GLU 80[O]
15	ASP 33[N]	3.20	ARG 83[O]
16	THR 96[OG1]	2.71	GLY 94[O]
17	THR 96[N]	3.03	THR 96[OG1]
18	THR 96[OG1]	3.48	THR 96[OG1]
19	ARG 35[NH2]	3.36	ASN 99[O]
20	ARG 35[NH2]	2.90	ALA 100[O]
21	ARG 35[NH1]	3.00	SER 102[O]
22	ARG 35[NH2]	2.94	SER 102[O]
23	ASN 24[O]	2.94	ARG 76[N]
24	ASN 31[O]	2.77	SER 61[OG]
25	ASN 31[OD1]	3.23	GLY 58[N]
26	ASN 31[OD1]	2.75	GLY 59[N]
27	GLN 32[O]	3.61	ARG 82[NH2]
28	GLN 32 [OE1]	2.99	ARG 82[NE]
29	ASP 33[OD1]	2.75	ARG 83[NE]
30	ASP 33[OD1]	3.05	TRP 85[NE1]
31	ASP 33[OD2]	2.81	ARG 83[NH2]
32	ASP 33[O]	2.76	ARG 83[N]
33	GLN 37[OE1]	3.35	ARG 83[NH1]
34	THR 56[O]	3.87	SER 29[OG]
35	THR 56[O]	2.99	ALA 30[N]
36	GLY 58[O]	3.86	ASN 31[ND2]
37	GLY 59[O]	2.50	ASN 31[ND2]
38	VAL 74[O]	2.90	ASN 24[N]
39	LEU 77[O]	2.88	SER 29[N]
40	GLU 80[O]	2.99	ARG 35[NE]
41	GLU 80[O]	2.81	ARG 35[NH1]
42	ARG 83[O]	3.13	ASP 33[N]
43	GLY 94[O]	2.66	THR 96[OG1]
44	THR 96[OG1]	3.09	THR 96[N]
45	ASN 99[O]	3.43	ARG 35[NH2]
46	ALA 100[O]	2.88	ARG 35[NH2]
47	SER 102[O]	3.02	ARG 35[NH1]
48	SER 102[O]	2.96	ARG 35[NH2]
Salt-bridge interactions			
1	LYS 69[NZ]	3.30	GLU 10[OE2]
2	ARG 71[NH1]	3.71	ASP 17[OD2]
3	LYS 30[NZ]	2.77	ASP 98[OD1]
4	LYS 30[NZ]	3.53	ASP 98[OD2]
5	GLU 10[OE2]	3.30	LYS 69[NZ]
6	ASP 17[OD2]	3.71	ARG 71[NH1]
7	ASP 98[OD1]	2.77	LYS 30[NZ]
8	ASP 98[OD2]	3.53	LYS 30[NZ]

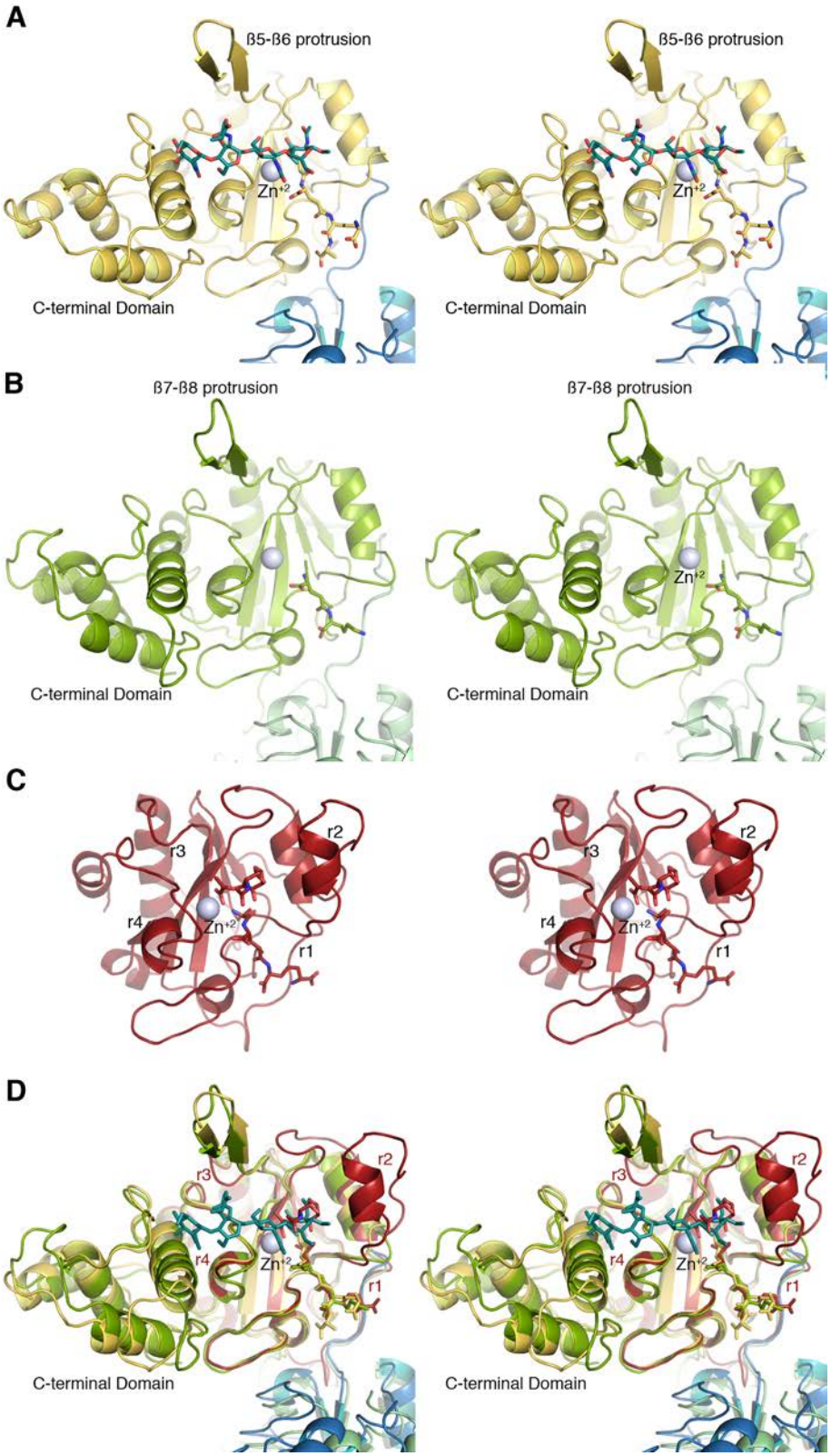

Figure S1. Ligand recognition in AmpDh2 (A), AmiD (B) and AmpD (C). As assessed by DALI server, [16] the closest structural homologues of AmpDh2 are AmiD, an amidase from *E. coli* (Z score 32.0, RMSD of 2 Å for 257 Cα atoms)[10] and the active conformation of the peptidoglycan-recycling amidase

AmpD from *Citrobacter freundii* (Z score 18.7, RMSD 1.6 Å for 176 Cα atoms).[17] (A) Three-dimensional structure of the AmpDh2:5P complex. The synthetic NAG-NAM-NAG-NAM (green sticks) observed in the AmpDh2:4S complex is superimposed to reveal the glycan-binding site. This is the first time a glycan chain is observed attached to a PG amidase. Monomer A and B are colored differently (yellow and blue, respectively). The reaction product (Ala-γ-D-Glu-*m*-DAP-D-Ala) is represented as yellow sticks. (B) Three-dimensional structure of *E. coli* AmiD-tripeptide complex.[10] The tripeptide is represented as green sticks. (C) The crystal structure of active AmpD from *C. freundii* in complex with the reaction products (anhydro-MurNAc and tripeptide, depicted as red sticks).[17] Activation observed in cytoplasmic AmpD involves large structural rearrangements (in both backbone and side chains) of the regions r2-r4, which are virtually unconnected through space to each other in the inactive form, but converge to come in close contact with one another in the active structure of AmpD.[17] The largest changes were observed in the r2 region. (D) Stereo view showing the structural superimposition of all related amidases. The C-terminal domain and the β5- β6 protrusion, involved in peptidoglycan recognition, are conserved in AmpDh2 and AmiD. Structural comparison with active of AmpD reveals that regions r2 and r3, key in the activation process, are absent in AmpDh2. The r4 region, critical to substrate stabilization, is conserved in AmpD and AmpDh2. The region r1 involved in stabilization of the terminal end of the peptide stem is absent in AmpDh2, but is replaced by the N-terminal segment from the dimeric partner.

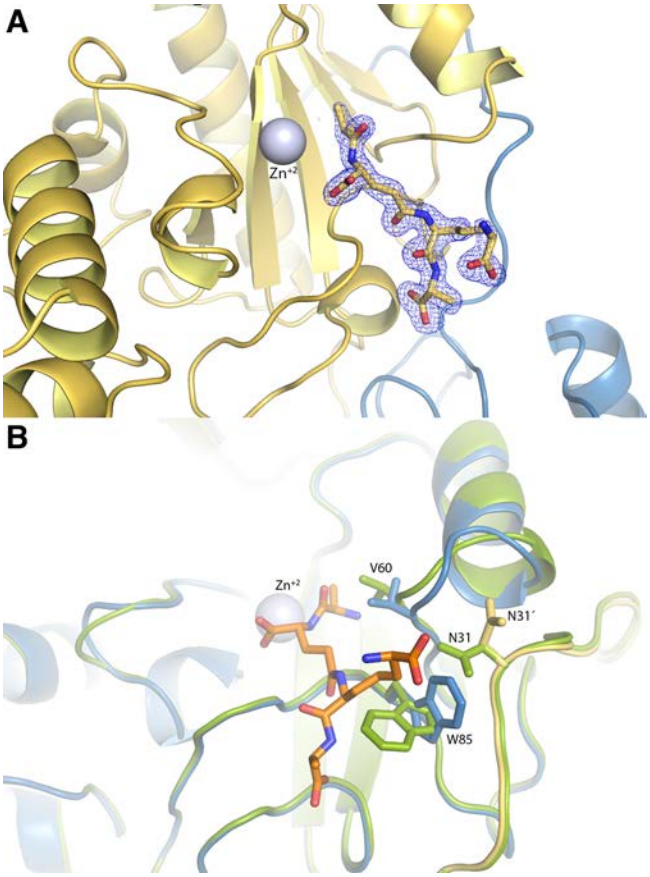

Figure S2. Tetrapeptide recognition by AmpDh2. (A) Electron density for the reaction product (Ala-γ-D-Glu-*m*-DAP-D-Ala) observed in the AmpDh2:5P complex. Electron density corresponds to the (2Fo-Fc) map contoured at 1σ. (B) Structural changes in AmpDh2 upon ligand binding. Apo AmpDh2 is colored in green and AmpDh2-product complex in blue (chain A) and in yellow (chain B). The ligand is represented in orange sticks. Residues with the most relevant changes are depicted in sticks.

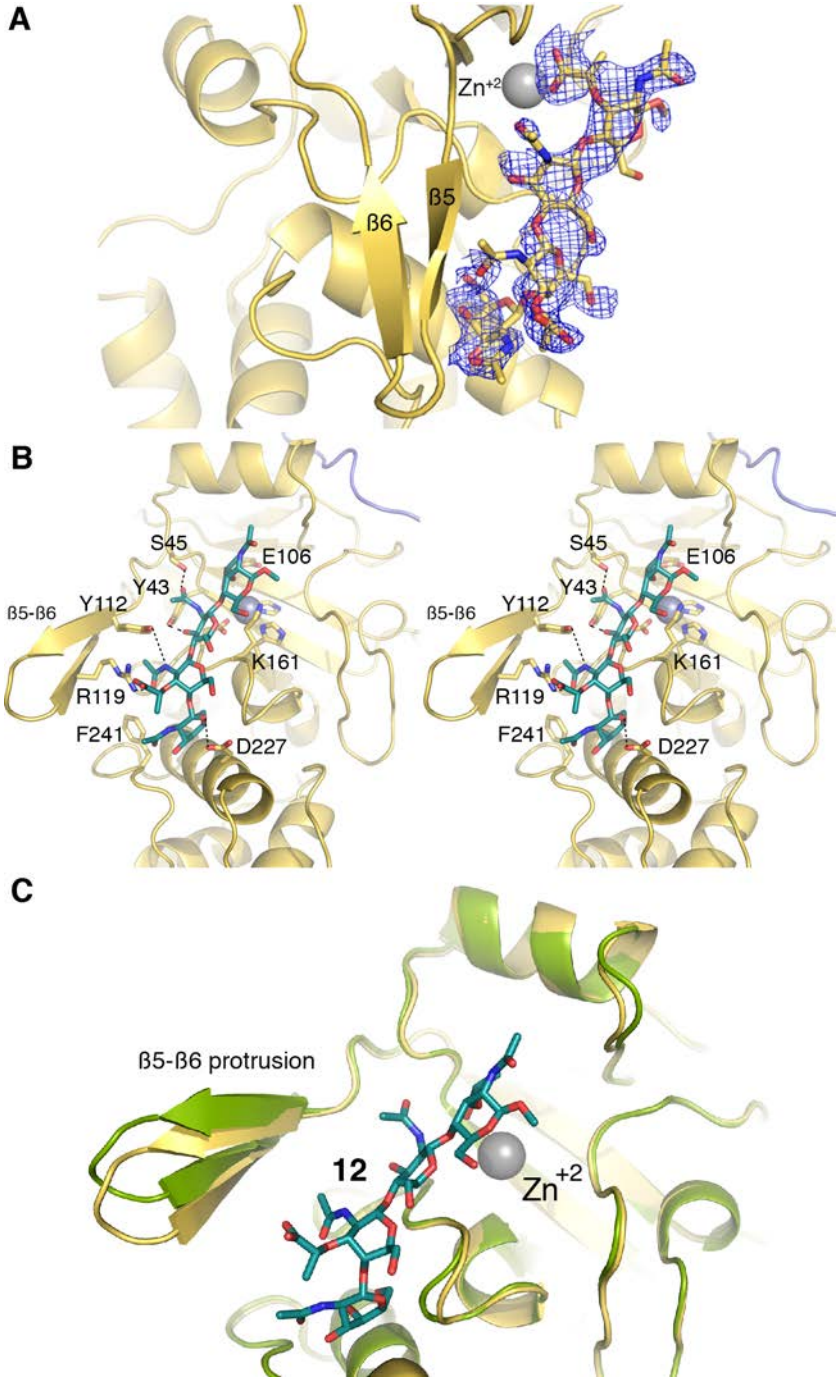

Figure S3. Tetrasaccharide **13** (β-methyl NAG-NAM-NAG-NAM) recognition by AmpDh2. (A) Electron density for the tetrasaccharide **13** observed in the AmpDh2:4S complex. Electron density corresponds to the (2Fo-Fc) map contoured at 0.8 σ. (B) Stereo view showing the tetrasaccharide (green sticks) at the glycan-binding site of AmpDh2. Relevant residues lining the cavity are drawn as yellow sticks. Catalytic zinc ion (gray sphere) and residues coordinating it are also depicted. (C) Structural changes in AmpDh2 upon tetrasaccharide binding. Apo AmpDh2 is colored in green and AmpDh2:4S complex in yellow. The β5-β6 protrusion clamps down on the substrate.

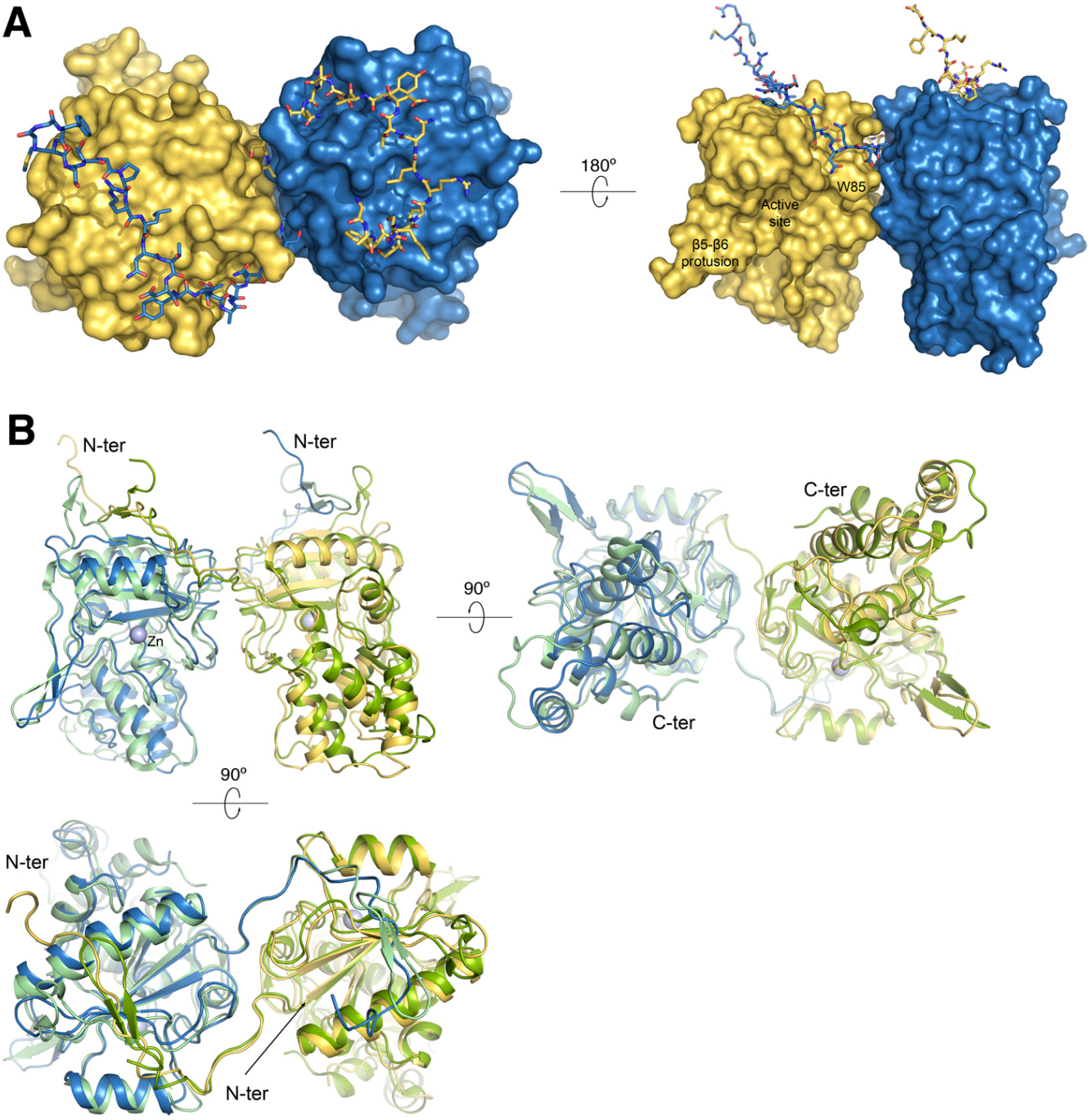

Figure S4. (A) Dimer arrangement in AmpDh2. Chain A is colored in yellow and chain B in blue. N-Terminal segment is represented as sticks and the remaining part as molecular surface. All the interactions involved in dimer formation are detailed in Table S2. (B) Comparison between oligomeric arrangement in AmpDh2 (colored as in panel A) and in *E. coli* AmiD (colored in green). In AmiD the asymmetric unit contains a single protein molecule, but AmiD forms a dimer with a symmetry-related molecule.[10] AmiD dimer follows the same structural arrangement observed for AmpDh2.

Sedimentation Velocity/Equilibrium Experiments

Sedimentation velocity (SV) data were fit with numerical solutions of the Lamm equation using SEDFIT.[2] Experimental SV data for AmpDh2 showed the presence of one species with an apparent mass (M_{app} = 58,000 ± 5000) consistent with a dimeric species (Figure S5A). The expected molecular weight of the dimer is 57,780 and the experimentally calculated M_{app} values are within the error of the calculated molecular weights. The experimentally obtained $s_{20,w}$ value for the corresponding dimeric species is 3.74 ± 0.25 (Figure S5B). The fitted SV experimental data with low residual error is also shown (Figure S5C). The data from sedimentation equilibrium (SE) experiments were best fit to a single-species model using the molecular weight of the AmpDh2 as a dimer (Figure S6). The combined SV and SE results indicated that AmpDh2 exists as a dimer in solution.

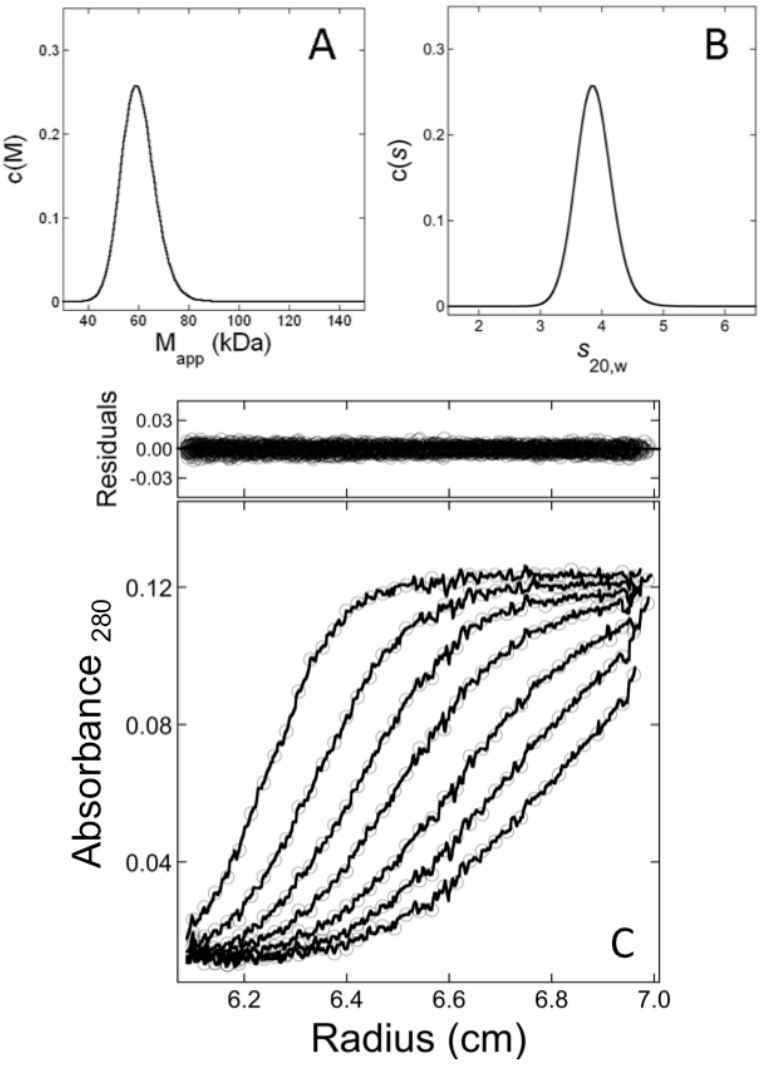

Figure S5. Sedimentation velocity analysis of AmpDh2 (3.1 μM) in 20 mM sodium phosphate, 0.1 M sodium chloride, pH 7.1, at 25,000 rpm at 4 ºC. (A) Experimentally obtained apparent molecular weights for AmpDh2 under above conditions. (B) Experimentally obtained *s* values converted to $s_{20,w}$ values for AmpDh2 under above conditions. (C) Plot shows a sample of experimentally obtained data fit to the Lamm equation using SEDFIT[2] and the residual values of the fitted data.

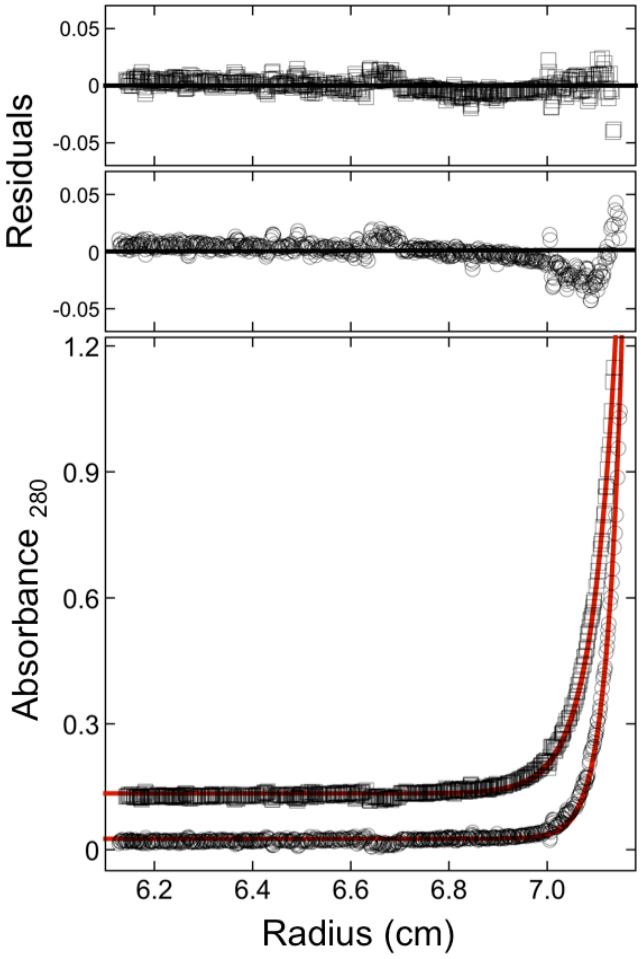

Figure S6. Sedimentation equilibrium analysis of AmpDh2 (4.9 μM) in 20 mM sodium phosphate, 0.1 M sodium chloride, pH 7.1, at 20,000 rpm (open squares) and 25,000 rpm (open circles) at 4 ºC. Plot shows a sample of experimentally obtained data for both rotor speeds fit to equation 2 and the residual values of the fitted data. The data for the 20,000 rpm was offset on the y axis for visual clarity.

Chart S2. Chemical Structures of the Products of the Sequential Reactions of AmpDh2 and of MltA with Pseudomonal Sacculus listed in Table S1.

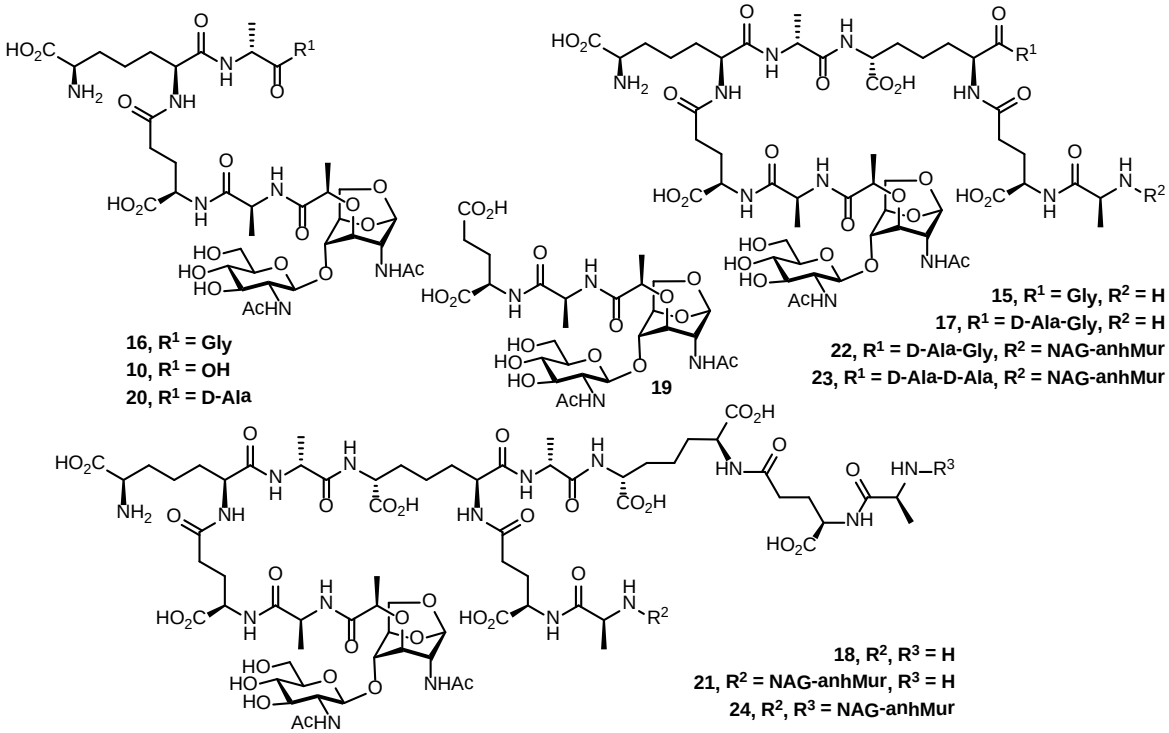

Table S3. The list of the products of the sequential reactions of AmpDh2 and of MltA with bacterial sacculus prepared from the stationary- and log-phase cultures.[a]

Name[b]		theoretical *m*/*z*	observed *m*/*z*	sacculus	
				Stationary-phase	Log-phase
NAG-anhMur	**1**	479.187^{+}	479.187^{+}	40%	65%
TriA1	**2**	851.352^{+}	851.353^{+}	4%	0.7%
	15	676.291^{2+}	676.292^{2+}	0.1%	ND[c]
TetraGlyA1	**16**	979.410^{+}	979.411^{+}	0.03%	ND[c]
	3	647.780^{2+}	647.785^{2+}	4%	1.6%
TetraA1	**10**	922.389^{+}	922.388^{+}	0.1%	1%
	17	711.810^{2+}	711.812^{2+}	0.2%	0.2%
	18	579.923^{3+}	579.921^{3+}	0.7%	0.5%
	4	683.299^{2+}	683.301^{2+}	37%	24%
DiA1	**19**	679.267^{+}	679.269^{+}	0.8%	1%
PentaA1	**20**	993.426^{+}	993.422^{+}	0.03%	ND[c]
	5	603.602^{3+}	603.601^{3+}	5%	7%
	21	1099.466^{2+}	1099.463^{2+}	0.2%	ND[c]
	6	1134.982^{2+}	1134.981^{2+}	2%	1%
TriTetraA2	**7**	877.865^{2+}	877.864^{2+}	1%	ND[c]
Tetra2GlyA2	**22**	941.894^{2+}	941.891^{2+}	0.1%	ND[c]
Tetra2A2	**8**	913.384^{2+}	913.382^{2+}	3%	ND[c]
TetraPentaA2	**23**	948.902^{2+}	948.901^{2+}	0.2%	ND[c]
TriTetra2A3	**24**	886.703^{3+}	886.706^{3+}	0.1%	ND[c]
Tetra3A3	**9**	910.382^{3+}	910.381^{3+}	0.3%	ND[c]
				1	0.22[d]
			Products	40%	65%
			Partially hydrolyzed products	49%	33%
			Unreacted substrates	11%	2%

[a] Amounts are expressed as a percentage of the overall peak area; ; [b] Naming conventions are based on the literature[4]; [c] ND, not detected; [d] the total peak area of products found for log-phase sacculus normalized to that of stationary-phase sacculus.

Structure elucidation of partial reaction products by LC/MS/MS. For the chromatographic peak that eluted at 15.2 minutes, the high-resolution accurate *m/z* value was found to be 683.301, which corresponds to the chemical formula $C_{55}H_{88}N_{12}O_{28}$. This chemical formula matches two possible structures (**4a** and **4,** see Figure S7A) of the crosslinked octapeptide with one unit of NAG-1,6-anhMur attached to either terminal alanine. Structure **4a** has the dissacharide attached to the acceptor end, while **4** has the dissacharide attached to the donor end. These two structures can be distinguished by their collisionally induced dissociation (CID) mass spectra. For example, only CID of protonated **4a** can generate product ions at *m*/*z* 993, *m*/*z* 790, *m*/*z* 922, and *m*/*z* 719. On the other hand, only CID of protonated **4** can generate product ions at *m*/*z* 904, and *m*/*z* 701. Because compound **8** (see Figure S7B) contains both arrangements of the disaccharide (as in **4** and **4a**) in one molecule, it was used as a reference to confirm that these CID product ions were generated from this structure. Indeed, the CID mass spectrum of protonated compound **8** showed product ions at *m*/*z* 993, *m*/*z* 790, *m*/*z* 922, and *m*/*z* 719 originated from the **4a** component, and *m*/*z* 904 and *m*/*z* 701 originated from the **4** component (Figure S7B). By comparison, the CID mass spectrum of the chromatographic peak, which eluted at 15.2 minutes revealed a product ion at *m*/*z* 701 (Figure S7A) like structure **4** and no product ions supporting **4a**. Therefore, we assign the predominant species of the 15.2-min eluting peak as **4**. Other observed product ions, which can be generated from both **4a** and **4**, were formed by the concomitant losses of saccharide(s), lactate, alanine, glutamate, diaminopimalate, and alanine (*i.e*. *m*/*z* 1162, *m*/*z* 977, *m*/*z* 834, *m*/*z* 705, *m*/*z* 533, and *m*/*z* 462).

Using the same approach as above, the structure of the 13.4-min chromatographic peak was determined. From the high-resolution accurate mass measurement of the *m*/*z* 647.785, the chemical formula $C_{52}H_{83}N_{11}O_{27}$ was deduced. This formula corresponds to the structure of the crosslinked heptapeptide with one unit of NAG-1,6-anhMur attached to one end of the peptide (**3a** and **3**, Figure S8A). CID of protonated **3a** can generate product ions at *m*/*z* 922, *m*/*z* 719, *m*/*z* 851, and *m*/*z* 648, while CID of protonated **3** can generate product ions at *m*/*z* 904 and *m*/*z* 701. To confirm the structure, the CID mass spectrum of **7** (Figure S8B) was used as a reference. Product ions at *m*/*z* 922, *m*/*z* 904, *m*/*z* 851, *m*/*z* 719, *m*/*z* 701, and *m*/*z* 648 were observed in the CID mass spectrum of protonated **7** (Figure S8B). The CID mass spectrum of the chromatographic peak that eluted at 13.4 minutes contained product ions at *m*/*z* 719 and *m*/*z* 701, which originated from both **3a** and **3**. Therefore, this chromatographic peak contains a mixture of the isobaric co-eluters **3a** and **3** (Figure S8A). Other observed product ions were formed by the concomitant losses of saccharide(s), lactate, alanine, glutamate, diaminopimalate, and alanine (*i.e*. *m*/*z* 1091, *m*/*z* 906, *m*/*z* 763, *m*/*z* 634, and *m*/*z* 462).

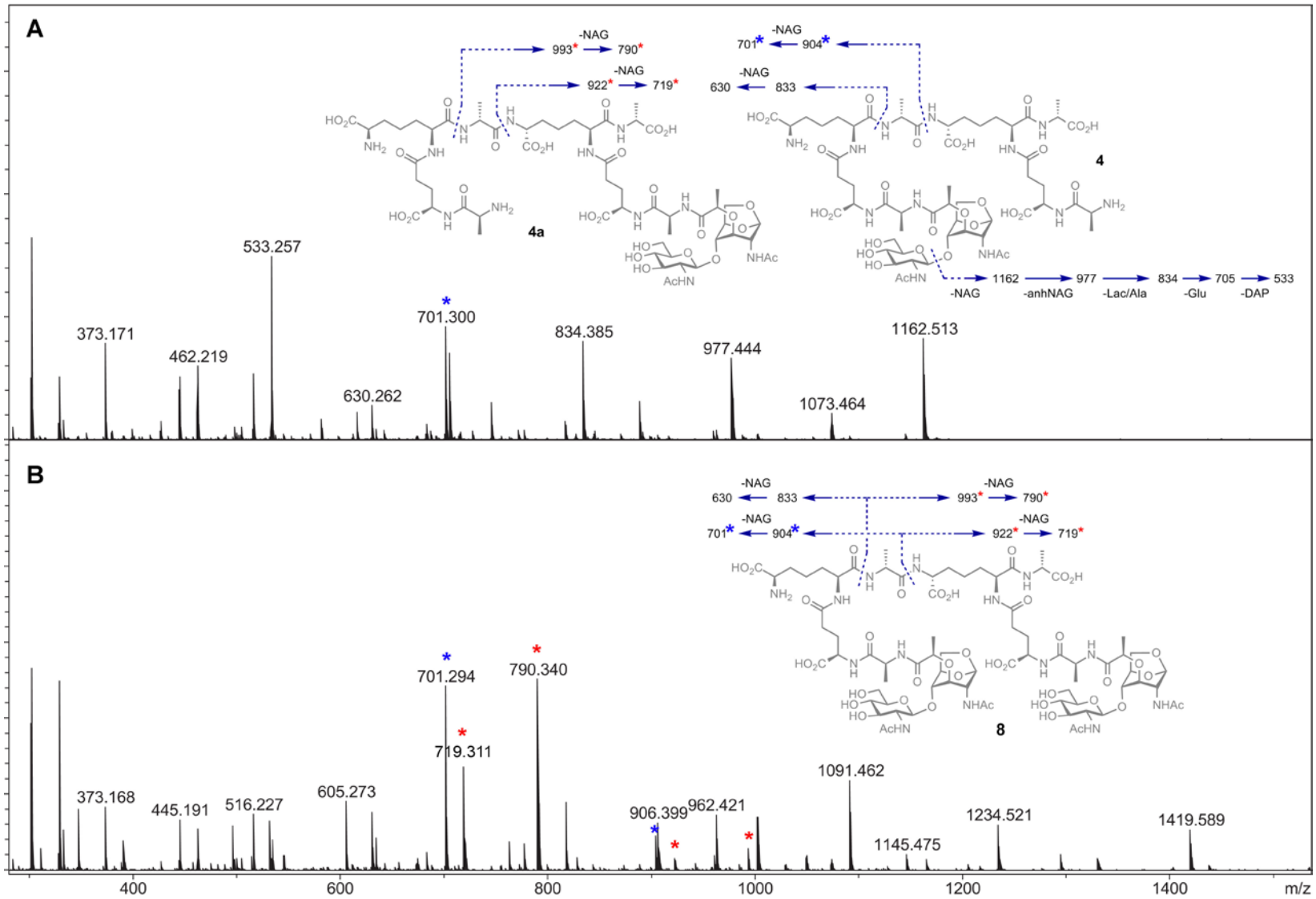

Figure S7. CID mass spectra of the partial-reaction products that eluted at 15.2 minutes (A) and compound **8** (B). Peaks representing unique fragment ions from protonated **4a** and protonated **4** are indicated by red and blue asterisk, respectively.

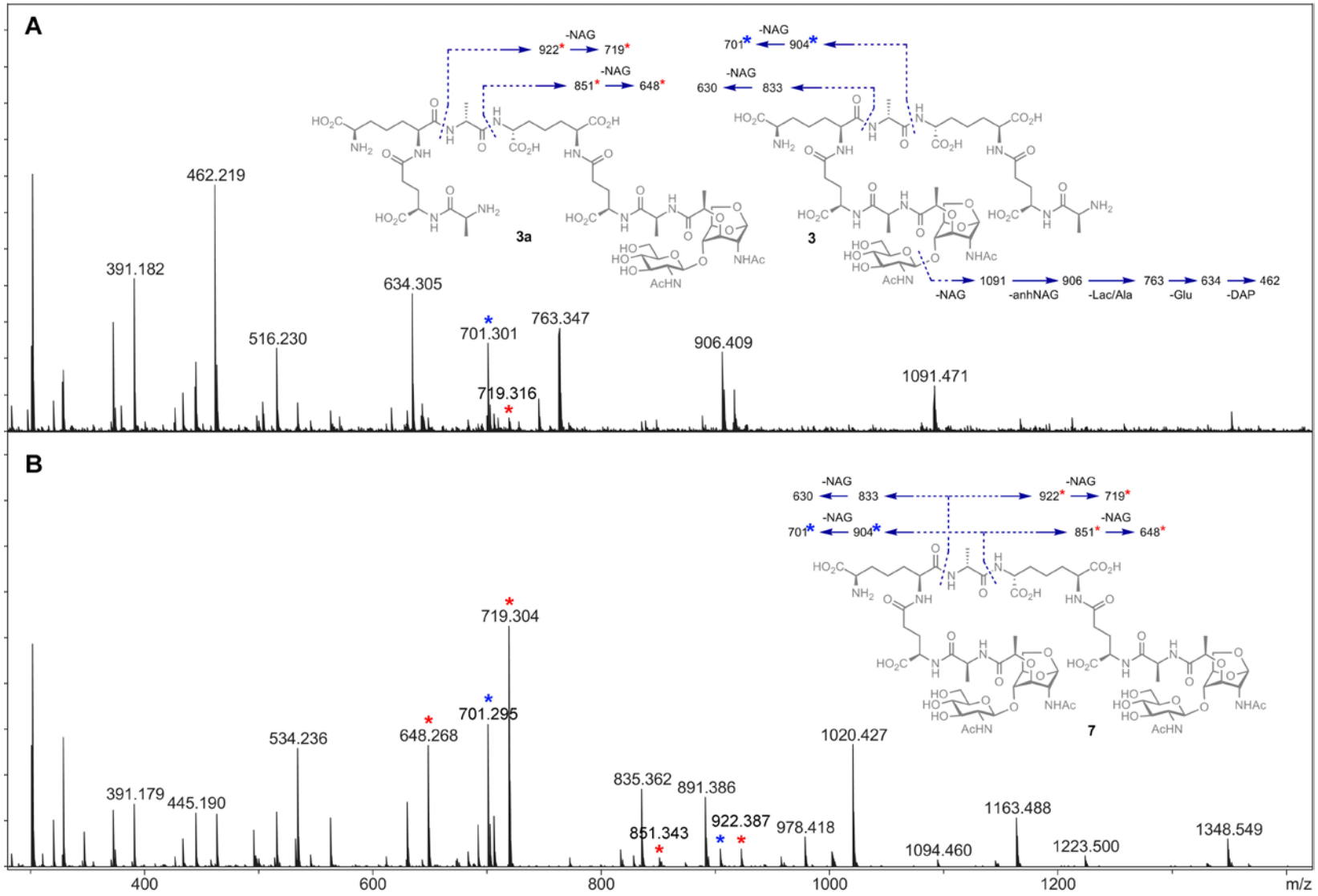

Figure S8. CID mass spectra of the partial-reaction products that elute at 13.4 minutes (A) and compound **7** (B). Peaks representing unique fragment ions from protonated **3a** and protonated **3** are indicated by red and blue asterisk, respectively.

References

(1) Zhang, W.; Lee, M.; Hesek, D.; Lastochkin, E.; Boggess, B.; Mobashery, S. *J. Am. Chem. Soc.* **2013**, *135*, 4950-4953.

(2) Schuck, P.; Perugini, M. A.; Gonzales, N. R.; Howlett, G. J.; Schubert, D. *Biophys. J.* **2002**, *82*, 1096-1111.

(3) Laue, T. M.; Shah, B. D.; Ridgeway, T. M.; Pelletier, S. L., Computer-aided interpretation of analytical sedimentation data for proteins. In *Analytical ultracentrifugation in biochemistry and polymer science*, Harding, S. E.; Rowe, A. J.; Horton, J. C., Eds.; The Royal Society of Chemistry: Cambridge, 1992; p 90–125.

(4) Lee, M.; Hesek, D.; Llarrull, L. I.; Lastochkin, E.; Pi, H.; Boggess, B.; Mobashery, S. *J. Am. Chem. Soc.* **2013**, *135*, 3311-3314.

(5) Lee, M.; Hesek, D.; Shah, I. M.; Oliver, A. G.; Dworkin, J.; Mobashery, S. *Chembiochem* **2010**, *11*, 2525-2529.

(6) Lee, M.; Zhang, W.; Hesek, D.; Noll, B. C.; Boggess, B.; Mobashery, S. *J. Am. Chem. Soc.* **2009**, *131*, 8742-8743.

(7) Hesek, D.; Lee, M.; Morio, K.-I.; Mobashery, S. *J. Org. Chem.* **2004**, *69*, 2137-2146.

(8) Kabsch, W. *Acta Crystallogr. D. Biol. Crystallogr.* **2010**, *D66*, 125-132.

(9) Collaborative Computational Project, N. *Acta Crystallogr. D. Biol. Crystallogr.* **1994**, *D50*, 760-763.

(10) Kerff, F.; Petrella, S.; Mercier, F.; Sauvage, E.; Herman, R.; Pennartz, A.; Zervosen, A.; Luxen, A.; Frère, J. M.; Joris, B.; Charlier, P. *J. Mol. Biol.* **2010**, *397*, 249-259.

(11) Emsley, P.; Cowtan, K. *Acta Crystallogr. D. Biol. Crystallogr.* **2004**, *D60*, 2126-2132.

(12) Afonine, P. V.; Grosse-Kunstleve, R. W.; Echols, N.; Headd, J. J.; Moriarty, N. W.; Mustyakimov, M.; Terwilliger, T. C.; Urzhumtsev, A.; Zwart, P. H.; Adams, P. D. *Acta Crystallogr. D. Biol. Crystallogr.* **2012**, *68*, 352-367.

(13) Vagin, A.; Teplyakov, A. *J. Appl. Crystallogr.* **1997**, *30*, 1022-1025.

(14) Adams, P. D.; Afonine, P. V.; Bunkoczi, G.; Chen, V. B.; Davis, I. W.; Echols, N.; Headd, J. J.; Hung, L. W.; Kapral, G. J.; Grosse-Kunstleve, R. W.; McCoy, A. J.; Moriarty, N. W.; Oeffner, R.; Read, R. J.; Richardson, D. C.; Richardson, J. S.; Terwilliger, T. C.; Zwart, P. H. *Acta Crystallogr. D. Biol. Crystallogr.* **2010**, *D66*, 213-221.

(15) Murshudov, G. N.; Skubák, P.; Lebedev, A. A.; Pannu, N. S.; Steiner, R. A.; Nicholls, R. A.; Winn, M. D.; Long, F.; Vagin, A. A. *Acta Crystallogr. D. Biol. Crystallogr.* **2011**, *D67*, 355-367.

(16) Holm, L.; Rosenström, P. *Nucleic Acids Res.* **2010**, *38*, W545-W549.

(17) Carrasco-López, C.; Rojas-Altuve, A.; Zhang, W.; Hesek, D.; Lee, M.; Barbe, S.; André, I.; Ferrer, P.; Silva-Martin, N.; Castro, G. R.; Martínez-Ripoll, M.; Mobashery, S.; Hermoso, J. A. *J. Biol. Chem.* **2011**, *286*, 31714-31722.